

# Dalton Transactions

Accepted Manuscript



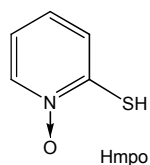
This is an *Accepted Manuscript*, which has been through the Royal Society of Chemistry peer review process and has been accepted for publication.

*Accepted Manuscripts* are published online shortly after acceptance, before technical editing, formatting and proof reading. Using this free service, authors can make their results available to the community, in citable form, before we publish the edited article. We will replace this *Accepted Manuscript* with the edited and formatted *Advance Article* as soon as it is available.

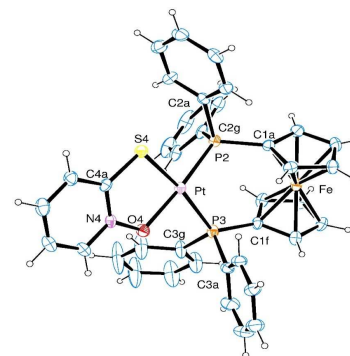
You can find more information about *Accepted Manuscripts* in the [Information for Authors](#).

Please note that technical editing may introduce minor changes to the text and/or graphics, which may alter content. The journal's standard [Terms & Conditions](#) and the [Ethical guidelines](#) still apply. In no event shall the Royal Society of Chemistry be held responsible for any errors or omissions in this *Accepted Manuscript* or any consequences arising from the use of any information it contains.

1,1'-bis(diphenylphosphino)ferrocene pyridine-2-thiolato-1-oxide Pd(II) and Pt(II) hexafluorophosphate compounds,  $[M(\text{mpo})(\text{dppf})](\text{PF}_6)$ , were synthesized and characterized. Both showed high cytotoxicity on *Trypanosoma cruzi* and *Mycobacterium tuberculosis* and good to excellent selectivity indexes towards *T. cruzi*. Experimental and molecular docking studies on modeled *T. cruzi* NADH-fumarate reductase showed that both are very good inhibitors of the parasite enzyme.



<b><math>[\text{Pd}(\text{mpo})(\text{dppf})](\text{PF}_6)</math></b>	<i>T. cruzi</i> : $\text{IC}_{50} = 0.64 \mu\text{M}$ <i>M. tuberculosis</i> : $\text{MIC} = 2.8 \mu\text{M}$ <i>Vero cells</i> : $\text{IC}_{50} 24 \mu\text{M}$
<b><math>[\text{Pt}(\text{mpo})(\text{dppf})](\text{PF}_6)</math></b>	<i>T. cruzi</i> : $\text{IC}_{50} = 0.28 \mu\text{M}$ <i>M. tuberculosis</i> : $\text{MIC} = 1.6 \mu\text{M}$ <i>Vero cells</i> : $\text{IC}_{50} 5 \mu\text{M}$



**Aromatic amine *N*-oxide organometallic compounds: searching for prospective agents  
against infectious diseases**

Esteban Rodríguez Arce,<sup>a</sup> M. Florencia Mosquillo,<sup>b</sup> Leticia Pérez-Díaz,<sup>b</sup> Gustavo A. Echeverría,<sup>c</sup> Oscar E. Piro,<sup>c</sup> Alicia Merlino,<sup>d</sup> E. Laura Coitiño,<sup>d</sup> Camila Maríngolo Ribeiro,<sup>e</sup> Clarice Q. F. Leite,<sup>e</sup> Fernando R. Pavan,<sup>e</sup> Lucía Otero,<sup>a\*</sup> Dinorah Gambino<sup>a\*</sup>

<sup>a</sup> Cátedra de Química Inorgánica, Departamento Estrella Campos, Facultad de Química, Universidad de la República, Gral. Flores 2124, 11800 Montevideo, Uruguay

<sup>b</sup> Laboratorio de Interacciones Moleculares, Facultad de Ciencias, Universidad de la República, Iguá 4225, 11400 Montevideo, Uruguay

<sup>c</sup> Departamento de Física, Facultad de Ciencias Exactas, Universidad Nacional de La Plata and Institute IFLP (CONICET, CCT-La Plata), C. C. 67, 1900 La Plata, Argentina

<sup>d</sup> Laboratorio de Química Teórica y Computacional, Instituto de Química Biológica, Facultad de Ciencias, Universidad de la República, Iguá 4225, 11400 Montevideo, Uruguay.

<sup>e</sup> Faculdade de Ciências Farmacêuticas, Unesp, 14801-902 Araraquara (SP), Brazil

\* To whom correspondence should be addressed. E-mail: [dgambino@fq.edu.uy](mailto:dgambino@fq.edu.uy);

[luotero@fq.edu.uy](mailto:luotero@fq.edu.uy); Tel. +5982-9249739; fax: +5982-9241906

**Keywords:** *Mycobacterium tuberculosis*; *Trypanosoma cruzi*; pyridine-2-thiol 1-oxide; ferrocene compounds; palladium and platinum

## Abstract

Searching for prospective agents against infectious diseases, 1,1'-bis (diphenylphosphino) ferrocene pyridine-2-thiolato-1-oxide M(II) hexafluorophosphate compounds  $[M(\text{mpo})(\text{dppf})](\text{PF}_6)$ , where M(II) = palladium or platinum, were synthesized and fully characterized in the solid state and in solution using experimental and DFT computational techniques. The compounds are isomorphous and the M(II) transition metal ions are in a nearly planar trapezoidal *cis*-coordination bound to the pyridine-2-thiolato-1-oxide (mpo) and to the 1,1'-bis (diphenylphosphino)ferrocene molecules, both acting as bidentate ligands. Both compounds showed high cytotoxic activity on *Trypanosoma cruzi* and *Mycobacterium tuberculosis* (MTB) and acceptable selectivities towards MTB, but good to excellent selectivity index values as anti-*T. cruzi* compounds. The inclusion of the ferrocene moiety (dppf ligand) improved the selectivity towards the parasite when compared to the previously reported  $[M(\text{mpo})_2]$  complexes. Related to the probable mechanism of action of the complexes, molecular docking studies on modeled *T. cruzi* NADH-fumarate reductase (*TcFR*) predicted that both should be very good inhibitors of the enzyme. The effect of the compounds on the enzyme activity was experimentally confirmed using *T. cruzi* protein extracts. According to all obtained results, both  $[M(\text{mpo})(\text{dppf})](\text{PF}_6)$  compounds could be considered prospective anti-trypanosomal agents that deserve further research.

## Introduction

Infectious diseases caused by pathogenic microorganisms such as bacteria, viruses, parasites or fungi, are the most prevalent illnesses worldwide and constitute an on-going threat to global health security.<sup>1</sup> Among them, Chagas disease (American trypanosomiasis) is a potentially life-threatening illness caused by the protozoan parasite *Trypanosoma cruzi* (*T. cruzi*) and

transmitted to the human host by infected triatomine bugs. It is an ancient, endemic disease in Latin America. It originally affected people living in rural areas where environmental conditions favor the installation of the bug. However, rural exodus, deforestation and urbanization have rendered it to a urban or peri-urban illness.<sup>2</sup> Currently, Chagas disease has spread to non-endemic countries in other continents mainly because of growing migratory flows. Globally, more than 10 million people are infected worldwide, mostly in Latin America. Only two old drugs are available for the treatment of the disease, namely Nifurtimox and Benznidazole. Both are poorly tolerated and show controversial efficacy. Hence the development of more efficacious and less toxic drugs is urgently needed.<sup>2-6</sup>

Tuberculosis (TB) is a highly contagious infectious disease caused by *Mycobacterium tuberculosis* (MTB). Although curable and preventable, it remains one of the leading causes of death in the world. In 2013, 9 million people felt ill and 1.5 million died from the disease. Over 95% of these deaths occurred in low- and middle-income countries. The risk of infection is higher in persons with impaired immune system; TB is a leading killer of HIV-positive people. About one-third of the world's population is infected but is not yet ill, bearing latent TB, working as reservoir of the disease.<sup>7,8</sup> Only few drugs are active against *M. tuberculosis* bacilli. Moreover, there is an increasing emergence of multi-drug resistant (MDR) and extensively drug resistant (XDR) MTB strains.<sup>9-12</sup>

Our group has been particularly devoted to the search for prospective metal-based drugs against *T. cruzi* and, more recently, *M. tuberculosis*.<sup>13-19</sup> In the case of anti-trypanosomal agents the main design strategy has consisted in the metal complexation of anti-parasitic organic compounds in an attempt to modulate their activity and global biological properties.<sup>13,14</sup> In this sense, some of us have been studying the effect of metal coordination on the bioactivity of the aromatic amine *N*-oxide, pyridine-2-thiol 1-oxide (Figure 1, Hmpo).<sup>16,20-22</sup>

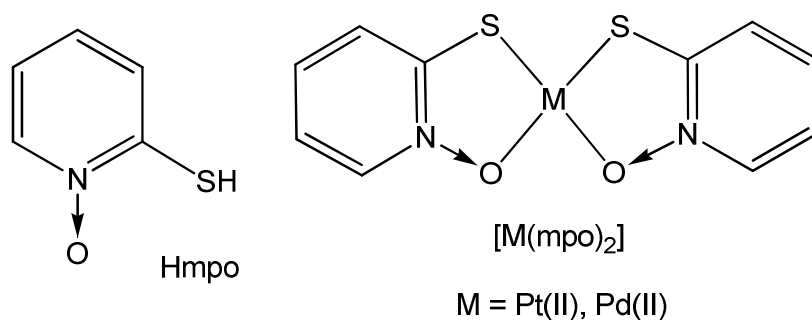


**Figure 1.** Pyridine-2-thiol 1-oxide (Hmpo, left) and its Pt(II) and Pd(II) complexes ( $[M(mpo)_2]$ , right).

Square planar complexes  $[M^{II}(mpo)_2]$ , where  $M(II) = Pd(II)$  or  $Pt(II)$  (Fig. 1) and the Au(I) homodinuclear mixed-ligand complex,  $[Au^I_2(mpo)_2(PPh_3)_2]$ , showed high activity on *T. cruzi*. Although they may have other intraparasite targets, the free ligand and the metal complexes inhibit the activity of the parasite specific enzyme NADH-fumarate reductase (*TcFR*), which is responsible for the conversion of fumarate to succinate as energy source. Whereas *TcFR* is essential for the survival of *T. cruzi*, being present in all the life cycle stages of the parasite, its absence in the human host makes it a promising target for selective anti-trypansomal drugs.<sup>20-21,23</sup>

Generation of succinate through a similar enzymatically catalyzed process has also been described in latent TB lung granulomas where the oxygen amount is severely limited. The use of the produced succinate enables MTB to maintain its basic physiological functions.<sup>24</sup> Accordingly, previously established mpo complexes with Bi(III), Fe(III) and Ga(III) showed to be potent anti-*M. tuberculosis* prospective agents.<sup>16</sup>

Among the previously developed mpo anti-trypansomal metal compounds, the  $[M(mpo)_2]$  complexes, with  $M = Pd$  or  $Pt$ , demonstrated to be the most promising ones (Fig. 1).

Nevertheless, both showed only moderate selectivity towards *T. cruzi* in respect to mammalian

cell model (J774 macrophages).<sup>20</sup> In order to further address the therapeutic potential of these metal-mpo complexes, we rationally designed two new compounds including a ferrocene derivative (1,1'-bis(diphenylphosphino) ferrocene; dppf) in the metal coordination sphere. The “sandwich type” ferrocene moiety has shown high potentiality in the development of novel organometallic drugs. For instance, compounds including it, like the antitumoral ferrocifen and the antimalarial ferroquine, have entered the phase of clinical trials. Although being organometallics, ferrocene derivatives are usually stable in air and in solution and, in addition, they usually show low cytotoxicity and confer the molecules were they are included adequate lipophilicity for trespassing cell membranes.<sup>25-27</sup>

In this work, 1,1'-bis(diphenylphosphino) ferrocene pyridine-2-thiolato-1-oxide M(II) hexafluorophosphate compounds [M(mpo)(dppf)](PF<sub>6</sub>), where M(II) = palladium or platinum, were synthesized and fully characterized in the solid state and in solution. Both species were evaluated on *T. cruzi* and *M. tuberculosis* as well as on VERO epithelial cells taken as mammalian cell model. The inhibitory effect of the newly developed compounds against TcFR, was predicted by molecular docking studies conducted on a model structure of the enzyme previously constructed by some of us. In addition, the inhibition of TcFR activity by the compounds was experimentally confirmed on *T. cruzi* protein extracts.

## Experimental

**General considerations.** All common laboratory chemicals were purchased from commercial sources and used without further purification. Pyridine-2-thiol 1-oxide sodium salt (Na mpo) and 1,1'-bis(diphenylphosphine) ferrocene (dppf) were commercially available. [MCl<sub>2</sub>(dppf)] precursors were synthesized according to a previously reported procedure by heating for 30 min an equimolar mixture of [MCl<sub>2</sub>(dmsO)<sub>2</sub>] and dppf in CHCl<sub>3</sub>.<sup>28</sup>

**Chemical and physical measurements.** C, H, N and S analyses were carried out with a Thermo Scientific Flash 2000 elemental analyzer. Conductimetric measurements were done over time (7 days) at 25 °C in  $10^{-3}$  M DMSO solutions using a Conductivity Meter 4310 Jenway to determine the type of electrolyte and to assess the stability of the complexes in such medium.<sup>29</sup>

The FTIR absorption spectra ( $4000\text{-}300\text{ cm}^{-1}$ ) were measured as KBr pellets with a Shimadzu IR Prestige-21 instrument.  $^1\text{H}$  NMR and  $^{13}\text{C}$  NMR spectra were recorded in DMSO- $d_6$  at 30 °C on a Bruker DPX-400 instrument (at 400 MHz and 100 MHz, respectively). Homo-nuclear correlation experiments (COSY) and hetero-nuclear correlation experiments (2D-HETCOR), HSQC (hetero-nuclear single quantum correlation) and HMBC (hetero-nuclear multiple bond correlation), were carried out with the same instrument. Tetramethylsilane was used as the internal standard.  $^{31}\text{P}$  NMR spectra were recorded on a Bruker Advance 400 MHz spectrometer (at 160.984 MHz) equipped with a 5 mm multinuclear broad-band dual probehead, incorporating a z-gradient coil.  $^{31}\text{P}\{^1\text{H}\}$  spectra were calibrated respect to the external pattern  $\text{H}_3\text{PO}_4$  10% (0.0 ppm). Chemical shifts are reported in ppm. Electrochemical behaviour was studied by cyclic voltammetry. Cyclic voltammograms were obtained with an Epsilon Electrochemical Analyzer. A standard electrochemical three electrode cell of 10 mL volume completed the system. A glassy carbon electrode was employed as a working electrode. A platinum wire was used as counter electrode while a Ag/AgCl electrode was used as a reference electrode. Measurements were performed at room temperature in 1mM acetonitrile solutions of the complexes using tetrabutyl amonium hexafluorophosphate (c.a. 0.1 M) as supporting electrolyte. Solutions were deoxygenated *via* purging with nitrogen for 15 min prior to the measurements. A continuous gas stream was passed over the solution during the measurements.



**Syntheses of [M(mpo)(dppf)](PF<sub>6</sub>), where M = Pd(II) or Pt(II).** The complexes were synthesized by the following procedure: 50 mg of the precursor [MCl<sub>2</sub>(dppf)] (0.068 mmol [PdCl<sub>2</sub>(dppf)] or 0.061 mmol [PtCl<sub>2</sub>(dppf)]) were dissolved in 10 mL methanol. To this solution, an equimolar amount of Na mpo (10.2 mg for the Pd compound and 9.1 mg for the Pt compound) dissolved in 5 mL methanol was added. The mixture was shaken at room temperature for 1 h. The solution was evaporated up to 5 mL and then kept in a refrigerator for 24 h. After adding NaPF<sub>6</sub> dissolved in a minimal volume of methanol (11.39 mg, 0.068 mmol for Pd and 10.22 mg, 0.061 mmol for Pt) the solution was kept again in refrigerator during 24 hs. The Pd compound was isolated as a reddish brown solid and the Pt compound as a greenish brown one. Single crystals suitable for X-ray diffraction studies were obtained in both cases by slow diffusion of hexane into a dichloromethane solution of the compounds.

**[Pd(mpo)(dppf)](PF<sub>6</sub>).** Yield: 40mg, 63%. Found: C, 50.13; H, 3.45; N, 1.50; S, 3.43. Calc. for C<sub>39</sub>H<sub>32</sub>F<sub>6</sub>FeNOP<sub>3</sub>PdS: C, 50.26; H, 3.46; N, 1.50; S, 3.44.  $\Lambda_M$ (DMSO): 34.7 Scm<sup>2</sup>mol<sup>-1</sup>. <sup>1</sup>H-NMR:  $\delta$  = 7.92 (1H, d, H5 mpo), 7.86 (4H, m, PPh<sub>2</sub>), 7.68 (12H, m, PPh<sub>2</sub>), 7.63 (1H, H2 mpo), 7.52 (1H, H3 mpo), 7.50 (4H, m, PPh<sub>2</sub>), 7.17(1H, t, H4 mpo), 4.95 (2H, s, H<sub>a</sub> Cp), 4.80 (2H, s, H<sub>b</sub> Cp), 4.64 (2H, s, H<sub>c</sub> Cp), 3.90 (2H, s, H<sub>d</sub> Cp) ppm. <sup>13</sup>C-NMR:  $\delta$  = 154.9 (C1, mpo), 138.1 (C5, mpo), 132.1 (C3, mpo), 127.5 (C2, mpo), 120.1 (C4, mpo), 78.13 (C-P Cp), 78.01 (C-H<sub>a</sub> Cp), 75.85 (C-H<sub>b</sub> Cp), 74.48 (C-H<sub>c</sub>, C-H<sub>d</sub> Cp) ppm. <sup>31</sup>P-NMR:  $\delta$  = 37.2 (d, PPh<sub>2</sub>), 29.3(d, PPh<sub>2</sub>), -143.0 (sept, PF<sub>6</sub>) ppm.

**[Pt(mpo)(dppf)](PF<sub>6</sub>).** Yield: 31 mg, 50%. Found: C, 45.75; H, 3.17; N, 1.37; S, 3.15. Calc. for C<sub>39</sub>H<sub>32</sub>F<sub>6</sub>FeNOP<sub>3</sub>PtS: C, 45.90; H, 3.16; N, 1.37; S, 3.14.  $\Lambda_M$ (DMSO): 33.1 Scm<sup>2</sup>mol<sup>-1</sup>. <sup>1</sup>H-NMR:  $\delta$  = 7.92 (1H, d, H5 mpo), 7.82 (1H, H2 mpo), 7.81 (4H, m, PPh<sub>2</sub>), 7.67 (12H, m, PPh<sub>2</sub>), 7.57 (1H, H3 mpo), 7.50 (4H, m, PPh<sub>2</sub>), 7.14(1H, t, H4 mpo), 4.78 (2H, s, H<sub>a</sub> Cp), 4.76 (2H, s, H<sub>b</sub> Cp), 4.62 (2H, s, H<sub>c</sub> Cp), 4.00 (2H, s, H<sub>d</sub> Cp) ppm. <sup>13</sup>C-NMR:  $\delta$  = 151.8 (C1, mpo), 139.1

(C5, mpo), 132.1 (C3, mpo), 128.2 (C2, mpo), 120.7 (C4, mpo), 76.89 (C-H<sub>a</sub> Cp), 75.85 (C-H<sub>b</sub> Cp), 75.39 (C-H<sub>c</sub> Cp), 75.02 (C-H<sub>d</sub> Cp) ppm. <sup>31</sup>P-NMR:  $\delta$  = 21.6 (d, PPh<sub>2</sub>), 9.8 (d, PPh<sub>2</sub>), -143.0 (sept, PF<sub>6</sub>) ppm.

**X-ray diffraction study of [M(mpo)(dppf)](PF<sub>6</sub>), where M = Pd(II) or Pt(II).** The

measurements were performed on an Oxford Xcalibur Gemini, Eos CCD diffractometer with graphite-monochromated MoK $\alpha$  ( $\lambda=0.71073$  Å) radiation. X-ray diffraction intensities were collected ( $\omega$  scans with  $\vartheta$  and  $\kappa$ -offsets), integrated and scaled with CrysAlisPro<sup>30</sup> suite of programs. The unit cell parameters were obtained by least-squares refinement (based on the angular settings for all collected reflections with intensities larger than seven times the standard deviation of measurement errors) using CrysAlisPro. Data were corrected empirically for absorption employing the multi-scan method implemented in CrysAlisPro. The complexes are isomorphous to each other and their common structure was solved by direct methods with the SHELXS-97 program of the SHELX package<sup>31</sup> and the molecular model developed by alternated cycles of Fourier methods and full-matrix least-squares refinement with SHELXL-97 of the same suit of programs.

The hydrogen atom were positioned on stereo-chemical basis and refined with the riding model. Crystal data, data collection procedure, structure determination methods and refinement results are summarized in Table 1. Crystallographic structural data have been deposited at the Cambridge Crystallographic Data Centre (CCDC). Any request to the CCDC for this material should quote the full literature citation and the reference number CCDC 1035234 (Pd) and CCDC 1035235 (Pt).

**Table 1.** Crystal data and structure refinement results for the [M(mpo)(dppf)]PF<sub>6</sub> (M = Pd, Pt) isomorphous complexes.

	[Pd(mpo)(dppf)]PF <sub>6</sub>	[Pt(mpo)(dppf)]PF <sub>6</sub>
Empirical formula	C <sub>39</sub> H <sub>32</sub> F <sub>6</sub> FeNOP <sub>3</sub> PdS	C <sub>39</sub> H <sub>32</sub> F <sub>6</sub> FeNOP <sub>3</sub> PtS
Formula weight	931.88	1020.57
Temperature (K)	295(2)	295(2)
Wavelength (Å)	0.71073	0.71073
Crystal system	Monoclinic	Monoclinic
Space group	<i>P2<sub>1</sub>/c</i>	<i>P2<sub>1</sub>/c</i>
Unit cell dimensions		
a (Å)	10.345(2)	10.3631(5)
b (Å)	22.319(3)	22.363(1)
c (Å)	17.307(3)	17.3974(9)
β (°)	106.23(2)	106.240(6)
Volume (Å <sup>3</sup> )	3836.6(10)	3871.0(3)
Z, density (calculated, Mg/m <sup>3</sup> )	4, 1.613	4, 1.751
Absorption coefficient (mm <sup>-1</sup> )	1.089	4.224
F(000)	1872	2000
Crystal shape / color	Needle / purple	Needle / yellow
Crystal size (mm <sup>3</sup> )	0.399 x 0.042 x 0.027	0.259 x 0.048 x 0.036
θ-range (°) for data collection	3.00 to 26.00	2.99 to 26.00
Index ranges	-12 ≤ h ≤ 12, -26 ≤ k ≤ 27, -21 ≤ l ≤ 21	-12 ≤ h ≤ 12, -27 ≤ k ≤ 17, -21 ≤ l ≤ 21
Reflections collected	18298	17086
Independent reflections	7532 [R(int) = 0.1320]	7599 [R(int) = 0.0528]

Observed reflections [ $I > 2\sigma(I)$ ]	3308	5221
Completeness (%)	99.8 (to $\theta = 26.00^\circ$ )	99.8 (to $\theta = 26.00^\circ$ )
Absorption correction	Semi-empirical from equivalents	Semi-empirical from equivalents
Max. and min. transmission	0.9712 and 0.6707	1.000 and 0.851
Refinement method	Full-matrix least-squares on $F^2$	Full-matrix least-squares on $F^2$
Data / restraints / parameters	7532 / 0 / 478	7599 / 0 / 478
Goodness-of-fit on $F^2$	0.995	1.018
Final R indices <sup>a</sup> [ $I > 2\sigma(I)$ ]	R1 = 0.0761, wR2 = 0.1348	R1 = 0.0452, wR2 = 0.0730
R indices (all data)	R1 = 0.1826, wR2 = 0.1847	R1 = 0.0829, wR2 = 0.0864
Largest diff. peak and hole (e.Å <sup>-3</sup> )	1.157 and -0.716	1.244 and -0.822

$$^a R_1 = \frac{\sum ||F_o| - |F_c||}{\sum |F_o|}, wR_2 = \left[ \frac{\sum w(|F_o|^2 - |F_c|^2)^2}{\sum w(|F_o|^2)^2} \right]^{1/2}$$

### Biological studies

**Determination of anti-MTB Minimal Inhibitory Concentration (MIC).** The anti-MTB activity of the compounds was determined by the REMA (Resazurin Microtiter Assay) method.<sup>32</sup> Stock solutions of the tested compounds were prepared in DMSO and diluted in Middlebrook 7H9 broth (Difco) supplemented with oleic acid, albumin, dextrose and catalase (OADC enrichment - BBL/Becton-Dickinson), to obtain final drug concentration ranges of 0.09-25  $\mu\text{g/mL}$ .

Isoniazid was dissolved in distilled water and rifampicin in DMSO, and both were used as standard drugs. A suspension of MTB H<sub>37</sub>Rv ATCC 27294 was cultured in Middlebrook 7H9 broth supplemented with OADC and 0.05% Tween 80. The cultures were frozen at  $-80^\circ\text{C}$  in aliquots. After two days the CFU/mL (colony formation unit/mL) of aliquot was determined. The concentrations were adjusted by  $5 \times 10^5$  CFU/mL and 100  $\mu\text{L}$  of the inoculum were added to each well of a 96-well micro-plate together with 100  $\mu\text{L}$  of the compounds. Samples were set up in triplicate. The plates were incubated for 7 days at  $37^\circ\text{C}$ . Resazurin (solubilized in water)

was added (30  $\mu\text{L}$  of 0.01%). The fluorescence of the wells was read after 24 h with a TECAN Spectrafluor<sup>®</sup>. The MIC was defined as the lowest concentration resulting in 90% inhibition of growth of MTB.

***In vitro anti-Trypanosoma cruzi activity.*** *T. cruzi* epimastigotes of the Dm28c strain were maintained in exponential growth at 28 °C in liver infusion tryptose (LIT) medium complemented with 10 % (v/v) fetal calf serum (FCS). The effect on cell growth was analyzed incubating an initial concentration of  $1 \times 10^6$  cells  $\text{mL}^{-1}$  with various concentrations (from 0 to 6  $\mu\text{M}$ ) of the compounds for 5 days in 96 well plates. Compounds were added as stock DMSO solutions immediately after the preparation of these solutions. The final DMSO concentration in the culture media never exceeded 0.4 % (v/v) and had no effect by itself on the proliferation of the parasites.<sup>33,34</sup> For the succinate protection assays, epimastigotes were also cultured for 5 days in presence or absence of 5 mM succinate. The percentage of cell growth was followed by measuring the absorbance, *A*, of the culture at 595 nm and calculated as follows: % =  $(A_p - A_{0p}) / (A_c - A_{0c}) \times 100$ , where  $A_p = A_{595}$  of the culture containing the drug at day 5;  $A_{0p} = A_{595}$  of the culture containing the drug at day 0;  $A_c = A_{595}$  of the culture in the absence of any drug (control) at day 5;  $A_{0c} = A_{595}$  in the absence of the drug at day 0. Dose-response curves were recorded and the  $\text{IC}_{50}$  values (50 % inhibitory concentration) were determined. The results are presented as averages  $\pm$  SD (standard deviation) and correspond to assays performed in triplicates. Nifurtimox (Nfx) was used as the reference trypanosomicidal drug.

***Cytotoxicity assay.*** *In vitro* cytotoxicity assays were performed on VERO epithelial cells (ATCC CCL81). This lineage is widely used for phenotypic screening of drugs being regarded as a normal cell derived from normal epithelial tissue.<sup>35</sup> The cells were routinely maintained in DMEM complete medium supplemented with 10% heat inactivated fetal bovine serum (FBS) plus gentamicin (50 mg/L) and amphotericin B (2 mg/L) at 37 °C, in a humidified 5%  $\text{CO}_2$  atmosphere. After reaching confluence, the cells were detached and counted. For the

cytotoxicity assay,  $1 \times 10^5$  cells/mL was seeded in 200  $\mu$ L of complete medium in 96-well plates (NUNC™). The plates were incubated under the same conditions for 24 h to allow cell adhesion prior to drug testing. The compounds were dissolved in DMSO (5%) and subjected to two-fold serial dilution from 500 to 3.9  $\mu$ g/mL. The cells were exposed to the compounds at various concentrations for 24 h. Resazurin solution was then added to the cell cultures and incubated for 6 h. Cell respiration (as an indicator of cell viability) was detected by reduction of resazurin to resorufin whose pink color and fluorescence indicate cell viability. A persistent blue color of resazurin is a sign of cell death. The fluorescence measurements (530 nm excitation filter and 590 nm emission filter) were performed in a SPECTRA fluor Plus (Tecan) microfluorimeter. The IC<sub>50</sub> value was defined as the highest drug concentration at which 50% of the cells are viable relative to the control. Each test was set up in triplicate.

***T. cruzi* NADH-fumarate reductase activity measurements.** For TcFR activity quantification *T. cruzi* epimastigotes (Dm28c clone) were grown at 28 °C in liver infusion tryptose (LIT) medium supplemented with 10% heat inactivated fetal bovine serum (FBS). *T. cruzi* protein extracts were prepared from  $5 \times 10^7$  exponentially grown parasites as previously described.<sup>20</sup> Briefly, parasites ( $1 \times 10^7$ /mL) were harvested at 500xg and resuspended in MST buffer (0.23 M mannitol, 0.07 M sucrose, 5 mM Tris HCl, pH 7.4) supplemented with protease inhibitors tablets (SIGMAFAST Protease Inhibitor tablets, SIGMA). Epimastigotes were homogenized in the presence of 0.1% Triton X-100 and 200 mM KCl on ice using a Potter-Elvehjem Teflon-glass homogenizer to disrupt the cell membranes and extract the enzyme. The preparation was immediately used to spectrophotometrically test NADH-fumarate reductase activity as the fumarate-dependent rate of NADH oxidation at 340 nm (molar absorption

coefficient =  $6.22 \text{ mM}^{-1} \text{ cm}^{-1}$ ) using 250  $\mu\text{M}$  NADH in Buffer HEPES 30 mM pH 7.0 containing 125 mM KCl and 0.5 mM fumarate as previously described.<sup>36</sup>

### Computational modeling

**DFT characterization.** Electronic structure calculations on the crystallographic geometry of each  $[\text{M}(\text{mpo})(\text{dppf})]^+$  complex were conducted by applying the BP86 GGA density functional<sup>37,38</sup> with the 6-31+G(d) basis set for all the non-metallic atoms<sup>39,40</sup> and the LANL2DZ relativistic effective core potential and the associated basis set for all the metal atoms<sup>41</sup> (Pt/Pd/Fe). Natural atomic NPA charges and Wiberg bond indices were derived for each structure from Weinhold's Natural Bond Orbital (NBO) analysis.<sup>42,43</sup> All the calculations were performed with the suite of programs Gaussian09.<sup>44</sup>

**Molecular docking studies on *T. cruzi* NADH-fumarate reductase.** The crystallographic structures of both M-dppf-mpo complexes (after hydrogen atoms removal) and the 3D structure of the central domain of *T. cruzi* fumarate reductase previously predicted by some of us combining homology modeling/molecular dynamics simulations<sup>22</sup> were used here for conducting ligand-protein docking with AutoDock 4.2.<sup>45</sup> The binding site of both complexes into TcFR was predicted by flexible-ligand docking using a grid box of  $126 \times 126 \times 126$  points (0.650 Å spacing) centered on the macromolecule to cover the entire protein surface (blind docking). Gasteiger-Marsilli charges were used and parameters for Pt(II) and Pd(II) were included in AutoDock's parameters file ( $R_{ii}$  and  $\epsilon_{ii}$  values for Pt(II) were based on AutoDock parameters for transition metals,<sup>46</sup> a set of parameters developed by Divsalar *et al.* were used for Pd(II), with  $R_{ii} = 2.50 \text{ Å}$  and  $\epsilon_{ii} = 0.458 \text{ kcal/mol}^{47}$ ). A Lamarckian genetic algorithm with population size of 150 individuals and  $2.5 \times 10^6$  energy evaluations was applied for 50 search runs. Default values were employed for the rest of the parameters. Protein-ligand structures differing by less than 2.0 Å in root-square deviation were grouped in the same cluster, choosing

the conformation with lowest binding energy from the most populated cluster for further analysis.

## Results and discussion

### Syntheses and characterization of the complexes

Two new organometallic heterobimetallic compounds of the bioactive ligand pyridine-2-thiolato-1-oxide (mpo) with the formula  $[M(\text{mpo})(\text{dppf})](\text{PF}_6)$ , where  $M = \text{Pd}(\text{II})$  or  $\text{Pt}(\text{II})$ , were obtained with good purity and good yield and they were exhaustively characterized in the solid state and in solution.

### Characterization of the complexes in the solid state

Most relevant IR vibration bands of both complexes were assigned taking into account previous assignments performed on related mpo compounds (Table 2).<sup>16,20,21</sup> The  $\nu(\text{N-O})$ ,  $\delta(\text{N-O})$  and  $\nu(\text{C-S})$  bands shift upon coordination to the metal in agreement with the bidentate coordination of the ligand through the oxygen of the N-O group and the sulfur, as shown by the corresponding crystal structures.

**Table 2.** Tentative assignment of the main characteristic bands of  $[M(\text{mpo})(\text{dppf})](\text{PF}_6)$ . Bands for mpo sodium salt, were included for comparison.<sup>20</sup> (wave numbers in  $\text{cm}^{-1}$ )

	$\nu(\text{N-O})$	$\delta(\text{N-O})$	$\nu(\text{C-S})$
Nampo	1263 (s)	833 (s)	706 (s)
$[\text{Pd}(\text{mpo})(\text{dppf})](\text{PF}_6)$	1246 (m)	834 (vs)*	694 (m)
$[\text{Pt}(\text{mpo})(\text{dppf})](\text{PF}_6)$	1252 (m)	840 (vs)*	694 (m)

$\nu$ : stretching;  $\delta$ : bending; s: strong; m: medium; vs: very strong. \*superimposed with the strong  $\nu(\text{P-F})$  of the  $\text{PF}_6^-$  counterion.



**Crystal structure of isomorphous Pd-dppf-mpo and Pt-dppf-mpo complexes.** Single crystals suitable for X-ray diffraction studies were obtained for both 1,1'-bis(diphenylphosphino)ferrocene pyridine-2-thiolato-1-oxide M(II) hexafluorophosphate compounds, where M(II) is palladium or platinum (Pd-dppf-mpo and Pt-dppf-mpo). Figure 2 shows an ORTEP<sup>48</sup> drawing of the platinum complex and its intra-molecular bond distances and angles around the metal along with the corresponding ones of the isomorphous palladium complex are given in Table 3. For this pair of isomorphous compounds a change in the nature of M precludes comparing the strength of the interactions at each metal coordination sphere by direct comparison of the corresponding M-L bond lengths. Therefore, for reaching that goal, a selection of Wiberg bond indices (WBI) calculated on the corresponding crystal structure at the BP87/6-31+G(d) level of theory are also included in Table 3 (See the complete set of calculated data in the supplementary information, Tables S1 and S2).

The M(II) transition metal ions are in a *quasi*-planar trapezoidal environment [*rms* deviation of atoms from the best least squares plane is less than 0.054 Å], coordinated to a nearly coplanar pyridine-2-thiolato-1-oxide anion acting as a bidentate ligand through its sulfur [M-S bond distances of 2.293(2) Å for Pd and 2.303(2) Å for Pt] and oxygen atoms [M-O lengths of 2.059(6) Å for Pd and 2.071(4) Å for Pt], and to the 1,1'-bis (diphenylphosphino)ferrocene neutral moiety acting as a bidentate ligand through its phosphorus atoms along their free tetrahedral binding direction [M-P distances of 2.240(3) Å and 2.335(2) Å for Pd and 2.239(2) Å and 2.316(2) Å for Pt]. Higher WBI values were found for all the M-S/M-O/M-P coordinative interactions in the Pt(II) species in comparison to their counterparts in the Pd(II) one; a feature that confers less reactivity to the Pt-dppf-mpo compound.

A similar planar coordination around Pd(II) was previously reported for the related [Pd(dppf)Cl<sub>2</sub>] complex [Pd-P distances of 2.283(1) and 2.301(1) Å],<sup>49</sup> but with a less marked

asymmetry between the two Pd-P bonds with respect to Pd-dppf-mpo. Platinum-mpo binding in Pt-dppf-mpo complex agrees with the one observed in the *trans*-coordinated [Pt(mpo)<sub>2</sub>] planar compound [mean Pt-S and Pt-O bond distances of 2.270(3) and 2.007(3) Å, respectively].<sup>50</sup> Similarly, palladium-mpo binding in Pd-dppf-mpo complex agrees with that observed in [Pd(mpo)<sub>2</sub>] [mean Pd-S and Pd-O bond distances of 2.242(2) and 2.043(5) Å, respectively].<sup>51</sup> In both M-dppf-mpo complexes the dppf ligand shows the expected Archimedean pentagonal anti-prism conformation for the coordination around iron in the ferrocene group, with the 5-membered Cp rings staggered to each other [Fe-C distances in the range from 2.014(6) to 2.079(6) Å for Pt-dppf-mpo and from 2.016(9) to 2.068(9) Å for Pd-dppf-mpo]. Phosphorus-C(Ph) bond distances are in the 1.808(6)-1.821(6) Å interval, while P-C(Cp) lengths are slightly shorter [1.794(6) and 1.798(6) Å].

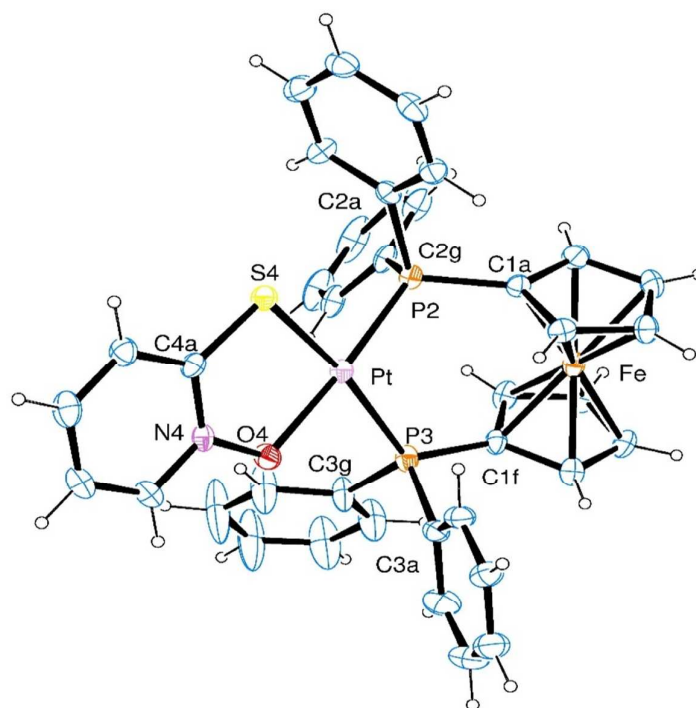


**Figure 2.** Drawing of platinum(II) complex in the [Pt(mpo)(dppf)]PF<sub>6</sub> solid showing the atomic displacement ellipsoids at the 20% probability level. For clarity, only a few representative atoms have been labeled and the PF<sub>6</sub> counter-ion has been omitted.

**Table 3.** Crystallographic bond lengths [Å] and angles [°] and DFT Wiberg bond indices<sup>a</sup> [a.u.] around the metal in the [M(mpo)(dppf)]PF<sub>6</sub> (M= Pd, Pt) compounds.

[Pd(mpo)(dppf)]PF <sub>6</sub>		[Pt(mpo)(dppf)]PF <sub>6</sub>	
Pd-O(4)	2.059(6) [ <i>0.39</i> ]	Pt-O(4)	2.071(4) [ <i>0.43</i> ]
Pd-P(2)	2.240(3) [ <i>0.66</i> ]	Pt-P(2)	2.239(2) [ <i>0.77</i> ]
Pd-P(3)	2.335(2) [ <i>0.58</i> ]	Pt-P(3)	2.316(2) [ <i>0.66</i> ]
Pd-S(4)	2.293(2) [ <i>0.66</i> ]	Pt-S(4)	2.303(2) [ <i>0.70</i> ]
O(4)-Pd-P(2)	174.9(2)	O(4)-Pt-P(2)	175.5(1)
O(4)-Pd-S(4)	84.4(2)	O(4)-Pt-S(4)	84.4(1)
P(2)-Pd-S(4)	91.73(9)	P(2)-Pt-S(4)	92.42(6)
O(4)-Pd-P(3)	87.0(2)	O(4)-Pt-P(3)	85.7(1)
P(2)-Pd-P(3)	97.03(9)	P(2)-Pt-P(3)	97.68(6)
S(4)-Pd-P(3)	170.9(1)	S(4)-Pt-P(3)	169.51(6)

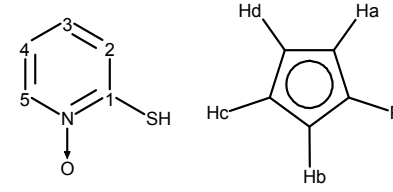
<sup>a</sup> values in italics between brackets.

### Characterization of the complexes in solution

No conductivity changes were observed during at least 7 days at 25°C. In addition, <sup>1</sup>H NMR spectra were measured during seven days. Neither changes in intensity of the signals nor new peaks due to release of free ligand were detected. Hence results suggest that the complexes are stable at air in DMSO solution.

## NMR results

**Table 4.**  $^1\text{H}$  NMR chemical shift values ( $\delta$ , in ppm) of the ligands and the complexes in  $\text{DMSO-}d_6$ .

				$\delta_{\text{H}}$ (multiplicity)(integration)		
Ligand	H	Free Ligand	$[\text{Pd}(\text{mpo})(\text{dppf})](\text{PF}_6)$	$\Delta\delta^a$	$[\text{Pt}(\text{mpo})(\text{dppf})](\text{PF}_6)$	$\Delta\delta^a$
Mpo	2	7.32 (d) (1)	7.63 <sup>(b)</sup> (1)	0.31	7.82 <sup>(b)</sup> (1)	0.50
	3	6.74 (t) (1)	7.52 <sup>(b)</sup> (1)	0.78	7.57 <sup>(b)</sup> (1)	0.83
	4	6.55 (t) (1)	7.17 (t)(1)	0.62	7.14 (t) (1)	0.59
	5	7.97 (d) (1)	7.92 (d) (1)	-0.05	7.92 (d) (1)	-0.05
Dppf (Cp ring)	H <sub>a</sub>	3.94 (s) (4)	4.95 (s) (2)	1.01	4.78 (s) (2)	0.84
	H <sub>d</sub>		3.90 (s) (2)	-0.04	4.00(s) (2)	0.06
	H <sub>b</sub>	4.27 (s) (4)	4.80 (s) (2)	0.53	4.76 (s) (2)	0.49
	H <sub>c</sub>		4.64 (s) (2)	0.37	4.62 (s) (2)	0.35
Dppf (PPh <sub>2</sub> )		7.23 (s) (8)	7.86 (m) (4)		7.81 (m) (4)	
			7.68 (m) (12)	-	7.67 (m) (12)	-
		7.34 (s) (12)	7.50 (m) (4)		7.50 (m) (4)	

<sup>a</sup>  $\Delta\delta = (\delta_{\text{complex}} - \delta_{\text{ligand}})$

<sup>b</sup> overlapped with PPh<sub>2</sub> protons

Multiplicity: s: singlet, d: doublet, t: triplet, m: multiplet

$^1\text{H}$ ,  $^{13}\text{C}$  and  $^{31}\text{P}$  NMR spectra were recorded to completely characterize the obtained complexes in  $\text{DMSO-}d_6$  solution. Two-dimensional NMR experiments such as COSY and HSQC aided in the assignment of the spectra. Results of the  $^1\text{H}$  NMR experiments for the ligands and the complexes are shown in Table 4. As expected, both complexes showed a similar pattern of signals corresponding to the protons of mpo and dppf ligands. Obtained integration and multiplicity are in accordance with the obtained stoichiometry of the complexes. A deshielding effect was observed on most of the protons as a consequence of metal coordination of mpo (which induces significant charge reorganization in the ligand, as can be appreciated from the changes in NPA atomic charge and WBI values collected in Table S2a). As previously observed for other mpo complexes,<sup>20,21</sup> protons **2** and **5**, respectively vicinal to the S and O coordinating atoms, were the less deshielded (actually, **2** was slightly shielded in both M-dppf-mpo complexes) due to back-donation of electron density from the S-M-O moiety. Two proton signals (singlets, four proton integration) at 3.94 and 4.27 ppm were observed for the Cp rings of the dppf free ligand. These signals have been assigned to equivalent Ha-Hd and Hb-Hc protons of both Cp rings that are coplanar to each other and with an average eclipsed conformation at room temperature (Table 4).<sup>52</sup> In the new compounds, these two signals split into four. The equivalence of the Cp protons is broken under formation of the M-dppf-mpo complexes due to the loss of fluxionality caused by the geometric requirements of the M-P bonding in the presence of the bidentate mpo ligand.<sup>53,54</sup> At higher ppm values, multiplets corresponding to protons of the  $\text{PPh}_2$  moieties were also observed.

Through 2D-HSQC experiments, the signals of the  $^{13}\text{C}$  NMR spectra could be partially assigned in spite of their observed complexity (Table S7). The most noticeable feature of the spectra is the change in the chemical shift of C1 carbon because of complexation

( $\Delta\delta = \delta_{\text{complex}} - \delta_{\text{ligand}} = -13.01$  and  $-16.11$  ppm for palladium and platinum compounds, respectively). This is in accordance with the  $^{13}\text{C}$  NMR spectroscopic behavior previously reported for other mpo complexes.<sup>16,20,21</sup>

$^{31}\text{P}$ -NMR spectra present two doublets corresponding to the  $\text{PPh}_2$  moieties at 37.2 and 29.3 ppm for the palladium compound and at 21.6 and 9.98 ppm for the platinum one. This clearly shows that the two phosphorus atoms are non-equivalent in the new complexes, in consistency with the crystallographic study and the asymmetries found in their NPA atomic charges (Table S2b) and the WBI indices for the chemical environment of each one in the M-dppf-mpo species (Table S1). For the platinum one, two satellites at the sides of the phosphorus signal due to the coupling with platinum atom were observed ( $J_{\text{PtP}} = 1605$  and  $1840$  Hz).<sup>55</sup> In addition, the typical septet at  $-143.0$  ppm corresponding to the  $\text{PF}_6^-$  counter ion was observed for both complexes.

### *Cyclic voltammetry studies*

The electrochemical properties of the complexes were investigated by cyclic voltammetry using a glassy carbon disc as working electrode, a platinum wire as counter electrode, and  $\text{Ag}/\text{AgCl}$  as reference electrode. Obtained voltammograms of the complexes (recorded at a potential scan rate of  $100$  mV/s in acetonitrile solution) are shown in Fig. 3.

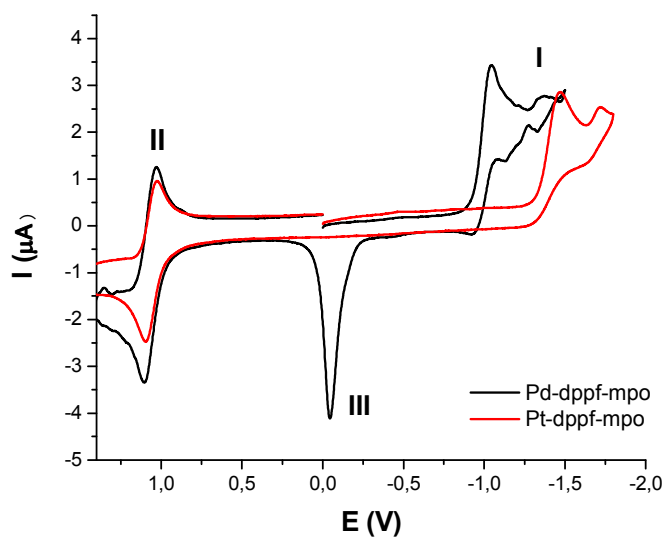


**Figure 3.** Cyclic voltammograms of the M-dppf-mpo (M=Pd, Pt) complexes at 100mV/s. Couple III corresponds to an adsorption process.<sup>56</sup>

Both complexes showed a similar electrochemical behaviour. On the forward cathodic scan, a reduction peak (I) was observed at -1.04 and -1.45 V for the palladium and platinum complexes, respectively. According to the behaviour previously reported for the  $[M(\text{mpo})_2]$  complexes with  $M = \text{Pd}$  or  $\text{Pt}$ , this peak could be assigned to the irreversible reduction of the metal center.<sup>20</sup> This is also consistent with the features of the corresponding Kohn-Sham LUMO orbitals ( $\sigma^*$  character, mainly involving  $M d_{x^2-y^2}$  contributions combined with  $p$ -orbitals from the P, O, S coordinative atoms at the two bidentate ligands, as shown in Fig. S1) obtained at the DFT level for the M-ddpf-mpo, with energies of -5.45 and -4.95 eV for  $M = \text{Pd}$  and  $\text{Pt}$ , respectively.

On the reverse scan, a reversible redox couple (II) characteristic of the  $\text{Fe}^{\text{III}}/\text{Fe}^{\text{II}}$  couple of the dppf ligand was observed at 1.07 and 1.06 V for the palladium and platinum complexes, respectively (again in agreement with the finding of HOMO KS orbitals –shown in Fig. S1- located on the ferrocenyl moiety for both compounds and very close in energy between them,

with values of -7.40 eV for the Pd and of -7.39 eV for the Pt species). The effect of the scan rate on the electrochemical response of this couple was investigated between 50 and 1000 mV/s. For both complexes the anodic and cathodic peak potentials ( $E_{pa}$  and  $E_{pc}$ ) were not dependent on the scan rate and the  $\Delta E_p$  values were around 60 mV. In addition, the  $ip_a/v^{1/2}$  value was invariant with changing scan rates and the ratio of cathodic to anodic peak currents ( $ip_c/ip_a$ ) remained near to unit (Fig. 4). This behaviour is expected for a reversible charge transfer process.<sup>57</sup>

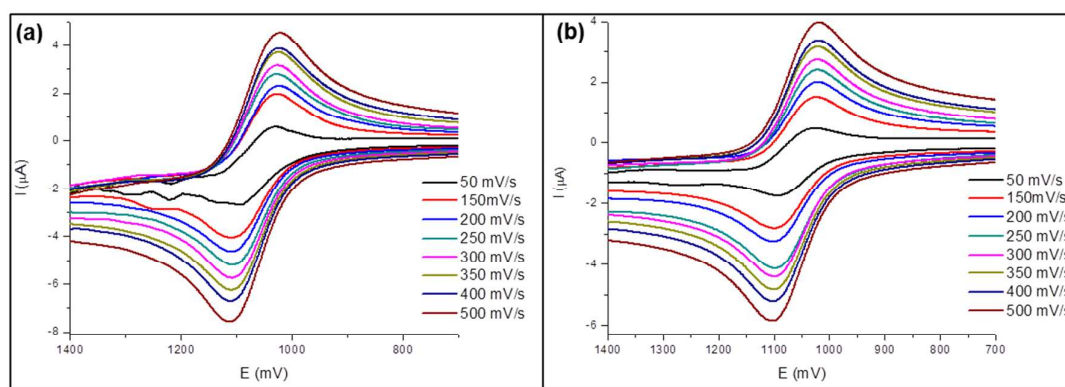


**Figure 4.** Cyclic voltammograms of M-dppf-mpo (M=Pd, Pt) complexes in the potential range of couple II at different scan rates: (a) Pd-dppf-mpo and (b) Pt-dppf-mpo.

### Biological results

***Anti-Mycobacterium tuberculosis activity.*** The metal compounds were evaluated in their activity on *Mycobacterium tuberculosis*, strain H<sub>37</sub>Rv ATCC 27294 (pan-susceptible). MIC values are collected in Table 5. Both species showed good to excellent activity against the bacillus when compared to the four first-line anti-TB drugs (MIC values: isoniazid 0.18  $\mu$ M, rifampicin 0.49  $\mu$ M, ethambutol 2.45  $\mu$ M, pyrazinamide 48.74  $\mu$ M), second-line anti-TB drugs, and some new molecules in clinical trials.<sup>16,58</sup> They displayed higher activity than some drugs already used in the treatment. The Pt compound resulted to be more active than the Pd



isostructural compound, reaffirming the important role played by the metal center in drug design, and also more active than Na mpo (MIC =  $2.42 \pm 0.07 \mu\text{M}$ ).<sup>16</sup>

**Table 5.** *In vitro* activity of M-dppf-mpo (M=Pd, Pt) complexes against *T. cruzi* (Dm28c epimastigotes), *M. tuberculosis* H<sub>37</sub>Rv ATCC27294, cytotoxicity on Vero epithelial cells (CCL81) and selectivity index (SI) values.

Compound	Vero cells	<i>M. tuberculosis</i>	SI (fold) <sup>a</sup>	<i>T. cruzi</i>	SI (fold) <sup>b</sup>
	IC <sub>50</sub> / $\mu\text{M}$	MIC / $\mu\text{M}$		IC <sub>50</sub> / $\mu\text{M}$	
Pd-dppf-mpo	24 $\pm$ 12	2.8 $\pm$ 0.7	9	0.64 $\pm$ 0.03	39
Pt-dppf-mpo	5 $\pm$ 3	1.6 $\pm$ 0.3	3	0.28 $\pm$ 0.01	18

<sup>a</sup> SI: IC<sub>50</sub> Vero cells / MIC *M. tuberculosis*. <sup>b</sup> SI: IC<sub>50</sub> Vero cells / IC<sub>50</sub> *T. cruzi*.

Results are the means of three different experiments.

***In vitro anti-Trypanosoma cruzi activity.*** The effect of both M-dppf-mpo compounds on the epimastigote form of *T. cruzi*, Dm28c strain, was evaluated and compared with that of Na mpo and the reference tripanosomicidal drug Nifurtimox. The results for the new compounds are shown in Table 5. Both showed high cytotoxic activity on the parasite with IC<sub>50</sub> values in the submicromolar range. A two- to five-fold increase of activity was observed with respect to free Na mpo (IC<sub>50</sub> =  $1.33 \pm 0.08 \mu\text{M}$ ) for Pd-dppf-mpo and Pt-dppf-mpo, respectively. In addition, the complexes showed about 10-20 times higher activity than the reference drug Nifurtimox (IC<sub>50</sub> =  $6.0 \mu\text{M}$ ).<sup>59</sup>

***Unselective cytotoxicity.*** In order to get further insight into the potentiality of both metal compounds as drugs, their corresponding cytotoxicity on VERO epithelial cells (ATCC CCL81) was assayed *in vitro*. The IC<sub>50</sub> values on these cells are shown in Table 5, together

with the selectivity index (SI) values calculated by dividing them by the MIC for *M. tuberculosis* H<sub>37</sub>Rv or by the IC<sub>50</sub> for *T. cruzi*, all of them expressed in  $\mu\text{M}$  units. Usually a compound is considered promising for further testing against *M. tuberculosis* if a SI value close or higher than 10 is found.<sup>60</sup> Thus from this study Pd-dppf-mpo emerges as a promising compound for further drug development.

Related to the *T. cruzi* selectivity, the new compounds showed very good SI values (Table 5). Even though compounds obtained in this work showed similar anti-*T. cruzi* activity than that of the previously developed [Pd(mpo)<sub>2</sub>] and [Pt(mpo)<sub>2</sub>] compounds ( $\text{IC}_{50[\text{Pd}(\text{mpo})_2]} = 0.067 \pm 0.015$ ,  $\text{IC}_{50[\text{Pt}(\text{mpo})_2]} = 0.200 \pm 0.018 \mu\text{M}$  on Tulahuen 2 strain)<sup>20</sup>, M-dppf-mpo ones were much less toxic ( $\text{SI}_{[\text{Pd}(\text{mpo})_2]} = 4.9$ ;  $\text{SI}_{[\text{Pt}(\text{mpo})_2]} > 10$ ; tested on J774 macrophages). In conclusion, although homoleptic and heteroleptic metal compounds showed similar activities, the inclusion of the ferrocene moiety seemed to decrease the cytotoxicity on mammalian cells increasing the selectivity against the parasite.

As pointed out by the aforementioned features of the “HOMO/LUMO” frontier KS orbitals of the new M-dppf-mpo species and their corresponding energy gaps (1.95 vs. 2.44 eV for M = Pd and Pt, respectively), whereas the palladium derivative appears as intrinsically more reactive and more prone to be reduced at the metal center M (in consistency with the comparative behaviour found for other Pd/Pt pairs of prospective square planar cytotoxic agents<sup>61,62</sup>) both species display the same tendency to undergo oxidation at the ferrocene moiety forming oxidized open-shell derivatives at the dppf ligand that could contribute to their biological action. Connected to the fact that Pt-dppf-mpo consistently displayed higher activity against both parasites and mammalian cells together with a lower selectivity, all these chemical features would be indicative of the involvement of multiple mechanisms and targets in the biological action of the M-dppf-mpo species. Whether production of cytotoxic radical species would be the main course of biological action, both compounds should in principle display

similar activity and unselective cytotoxicity patterns, which is not the case here, as shown by the data collected in Table 5. On the other hand, whether a chemical reaction involving ligand-exchange and/or reduction of M by biomolecular targets would be the main mechanism of action of these two new compounds, an unobserved higher activity should be expected for Pd-dppf-mpo, unless side-reactions with other components present in the biological assays (condition excluding *fumarate reductases*, which are not present in Vero cells, as the sole target of action) selectively capture the more reactive Pd species early before reaches its molecular target, thus explaining the observed modulation of activity/selectivity resulting by the change in the nature of the central metal M. The greater selectivity found against *T. cruzi*, makes it of special interest for further exploration of more specific mechanisms of anti-parasitic action, as the inhibition of *TcFR* addressed in the next section by a combination of biological and docking approaches.

***Interaction with TcFR: biological studies and molecular docking.*** Since we have previously shown that other mpo compounds inhibit fumarate reductase activity as part of their probable mechanism of antitrypanosomal action, we analyzed the effect of the newly developed Pd and Pt mpo complexes on this enzyme activity. Figure 5 shows the results of the inhibition test at a single dose (28  $\mu\text{M}$ ). In the conditions assayed, the free ligand and both metal-mpo complexes inhibited *T. cruzi*'s NADH-fumarate reductase activity. Both complexes showed a marked increase in the inhibitory effect respect to the free ligand, showing the Pt compound the highest inhibition. Interestingly a similar trend was observed when analyzing the  $\text{IC}_{50}$  of these metal compounds against *T. cruzi* epimastigotes.

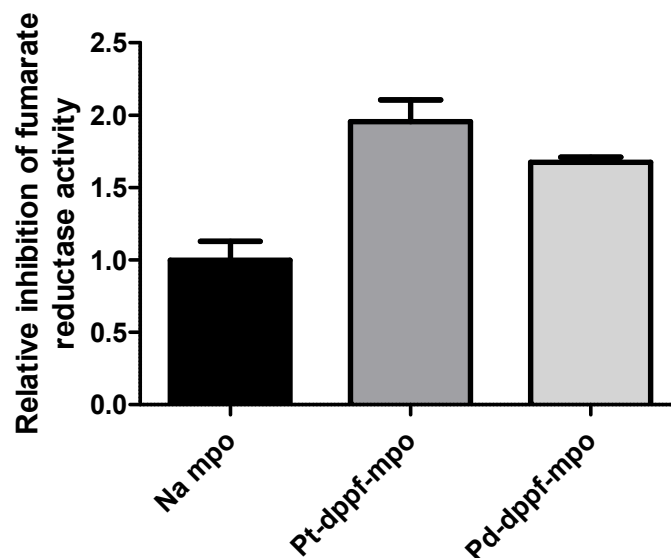


**Figure 5.** Inhibitory effect of metal-mpo complexes and Na mpo on *T. cruzi* NADH-fumarate reductase activity. Protein extracts of *T. cruzi* epimastigotes were incubated for 5 minutes at 30 °C in the absence (control) or presence of 28  $\mu$ M of Na mpo, Pt-dppf-mpo and Pd-dppf-mpo prior to the spectrophotometrical measurement of NADH-fumarate reductase activity as mentioned in Experimental. The total enzyme inhibition produced by Na mpo (■) was used to calculate the relative fold of inhibition produced by Pt-dppf-mpo (■) and Pd-dppf-mpo (■). S.D. for each compound is shown for two independent studies.

In order to further characterize the enzyme inhibition by both M-dppf-mpo complexes, the dependence of their inhibitory effect on concentration was studied. Pd-dppf-mpo and Pt-dppf-mpo inhibit the enzyme activity in a dose-dependent manner (Fig. 6).

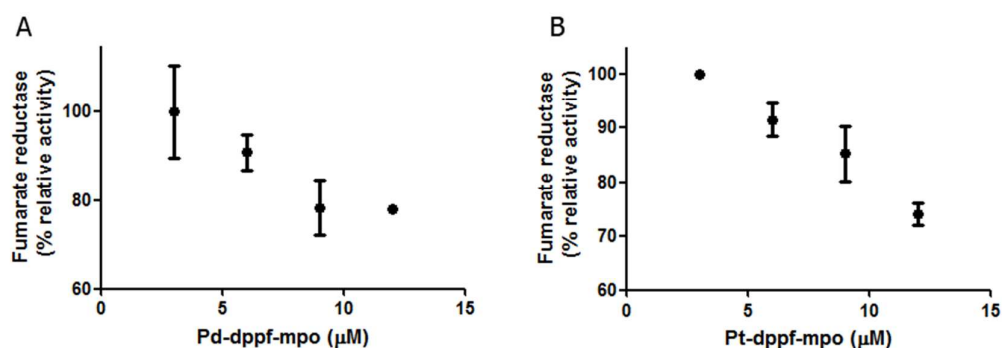


**Figure 6.** Inhibitory effect of Pd-dppf-mpo (A) and Pt-dppf-mpo (B) on NADH fumarate reductase activity from *T. cruzi* epimastigotes. Protein extracts were incubated with various concentrations of the complexes (3, 6, 9 and 12  $\mu\text{M}$ ) for 1 h at 28  $^{\circ}\text{C}$  prior to the spectrophotometrical measurement of NADH-fumarate reductase activity as described in Experimental. Average of two replicas is shown with their SD.

Since *TcFR* is the enzyme responsible for the conversion of fumarate to succinate, which is one of the main respiratory substrates required by the parasite for energy production,<sup>23</sup> we sought to analyze the protective effect of succinate in presence of the aforementioned compounds to analyze the involvement of *TcFR* as a target in their mechanism of action. The effect of succinate on parasite proliferation was analyzed as described in Experimental, by measuring absorbance at 595 nm at day 5 of incubation using Pt-dppf-mpo and Pd-dppf-mpo concentrations in the range of their  $\text{IC}_{50}$  values (0.3 and 0.6  $\mu\text{M}$ , respectively). The ability of succinate to protect the parasites from the effect of the compounds was evaluated in triplicates and in comparison with a control with no succinate. As shown in Fig. 7, a clear relief of the growth inhibition produced by the compounds was observed in the presence of added succinate in culture medium.

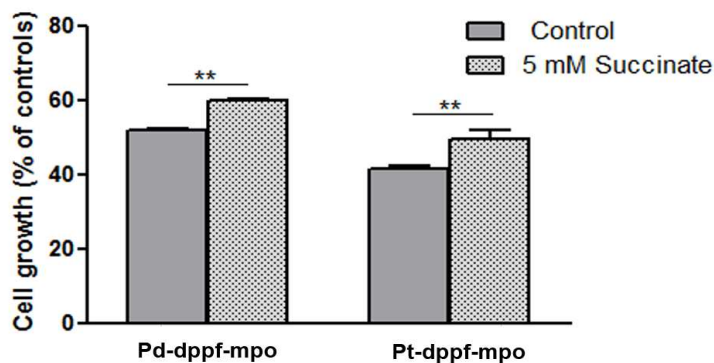


**Figure 7.** Protective effect of succinate against the inhibition of parasite growth caused by Pd-dppf-mpo and Pt-dppf-mpo. Epimastigotes were incubated with 0.6 and 0.3  $\mu\text{M}$  of Pd-dppf-mpo and Pt-dppf-mpo, respectively, in presence or absence of 5 mM succinate. The percentage of cell growth was plotted comparing both conditions: succinate (dotted pattern) or no added succinate (filled pattern). Averages of three replicas are shown with their SD values. \*\*: P values  $<0.01$  *t*-test.

Though we cannot discard that both metal-mpo complexes could be affecting other processes contributing to the blockage of *T. cruzi*'s growth, they clearly have an inhibitory effect on NADH-fumarate reductase activity.

Molecular docking shows that like the other Pt(II)- and Pd(II)-mpo complexes previously studied by our group,<sup>22</sup> both  $[\text{M}(\text{mpo})(\text{dppf})]^+$  species bind in a lobby cavity of the enzyme, close to the cofactor binding site (Fig. 8), and positioned next to residues Ser763 and Lys714. Since Ser763 is adjacent to the catalytic Arg762, such binding could affect the proper positioning of this residue for catalysis.

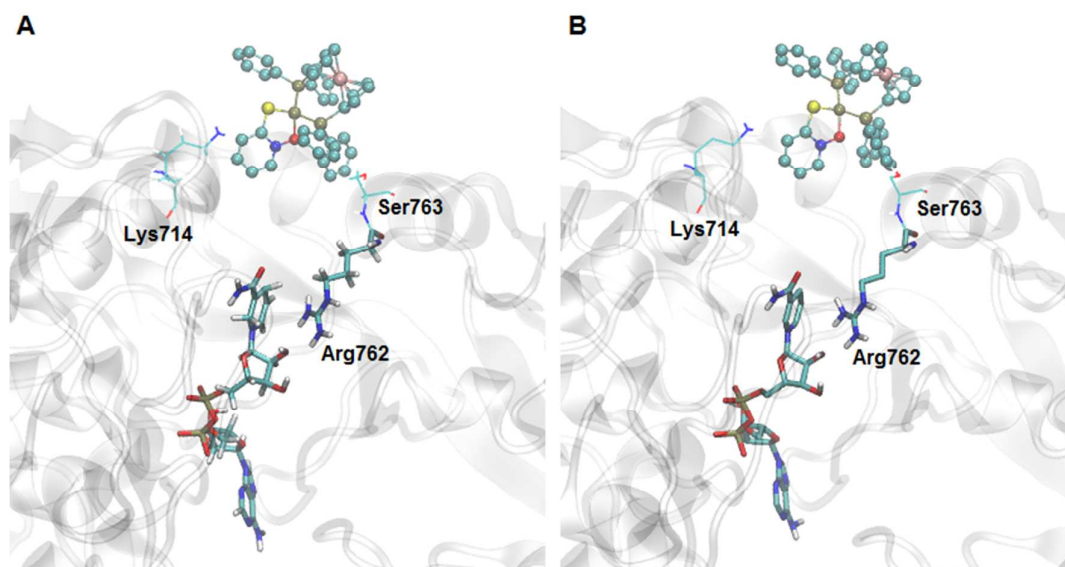


**Figure 8.** Predicted binding mode for Pt-dppf-mpo (**A**) and Pd-ddpf-mpo (**B**) into *TcFR*. The cofactor (NADH) and the catalytic Arg762 residue are shown in sticks representation. The metal complex is depicted in ball and sticks. Other residues in contact with the complex are shown in line representation.

Theoretical inhibition constants ( $K_i$ ) predicted by Autodock for these Pt and Pd derivatives are 4.5 and 2.3  $\mu\text{M}$ , respectively, indicating that both compounds would act as very good inhibitors of *TcFR*, in agreement with the experimental results on cellular extracts of the parasite. Up to now these derivatives containing a ferrocene moiety showed the lowest predicted  $K_i$  values against *TcFR* among the heteroleptic and homoleptic metal complexes considered here and in our previous study.<sup>22</sup>

All this evidence supports the strategy of introducing the dppf ligand for modulating the features of these species determines not only their anti-parasitic efficacy, but also their *TcFR* inhibition ability, making them promising leaders deserving further efforts in the design of more selective inhibitors against *T. cruzi*.

## Conclusions

Two new organometallic isomorphous platinum and palladium pyridine-2-thiolato 1-oxide compounds,  $[M^{II}(\text{mpo})(\text{dppf})](\text{PF}_6)$ , were synthesized and fully characterized in the solid state and in solution by experimental and computational techniques. Both showed high cytotoxic activity against *T. cruzi* and *M. tuberculosis*. In particular, they showed MIC values comparable to those of the four first-line anti-TB drugs and 10- to 20-fold higher antitrypanosomal activity than the drug Nifurtimox and 2- to 5-fold higher activity than the mpo ligand alone. The compounds showed acceptable selectivity index values as anti-TB compounds but good to excellent selectivity indexes as anti-*T. cruzi* agents. The inclusion of the ferrocene moiety (dppf ligand) improved the selectivity towards the parasite when compared to the previously reported  $[M(\text{mpo})_2]$  complexes. Molecular docking studies on modeled *T. cruzi* NADH-fumarate reductase predicted that both compounds should be very good inhibitors of the enzyme. This inhibitory effect was confirmed on *T. cruzi* protein extracts *in vitro*. Our results strongly suggest that the inhibition of the parasite-specific enzyme NADH-fumarate reductase could be an important part of the mechanism of trypanosomicidal action of the complexes. The generation of the recombinant NADH-fumarate reductase of *T. cruzi*, work currently in progress, would allow us to conduct experiments for assessing the inhibitory activity of these compounds on the pure enzyme specifically. According to the observed anti-*T. cruzi* activity and selectivity and molecular docking studies both  $[\text{Pt}(\text{mpo})(\text{dppf})](\text{PF}_6)$  and  $[\text{Pd}(\text{mpo})(\text{dppf})](\text{PF}_6)$  could be considered promising anti-trypanosomal agents and leaders for further efforts in the design of better and more selective inhibitors against *T. cruzi*.

## Acknowledgements

E.R.A. and F.M. acknowledge the support of the Agencia Nacional de Investigación e Innovación (ANII, Uruguay) through the grants POS\_NAC\_2013\_1\_11436 and



INI\_X\_2013\_1\_101093, respectively. This work was supported by CSIC-Universidad de la República (project 800) of Uruguay, CONICET (PIP 1529) and ANPCyT (PME06 2804 and PICT06 2315) of Argentina and Conselho Nacional de Desenvolvimento Científico e Tecnológico (CNPq/Glaxo ref. Process: 406827/2012-5), Coordenação de Aperfeiçoamento de Pessoal de Nível Superior (CAPES), Pró-Reitoria de Pesquisa/UNESP (PROPE ref. Process: 0102/004/43) and Fundação de Amparo à Pesquisa do Estado de São Paulo (FAPESP ref. Process: 2011/21232-1) of Brazil. G. A. E. and O. E. P are Research Fellows of CONICET.

**Supplementary Information Available.** KS HOMO and LUMO calculated features for both  $[M(\text{mpo})(\text{dppf})]^+$  complexes (Fig. S1). Table of calculated Wiberg bond indices (WBI) for the main bonding interactions in the  $[M(\text{mpo})(\text{dppf})]^+$  structures (Table S1). Tables of calculated NPA atomic charges for the mpo moiety in the  $[M(\text{mpo})(\text{dppf})]^+$  species and in the free ligand, and for the metal and dppf moiety in the  $[M(\text{mpo})(\text{dppf})]^+$  complexes (Tables S2a,b). Tables of fractional coordinates and equivalent isotropic displacement parameters of the non-H atoms (Tables S3a,b), full intra-molecular bond distances and angles (Tables S4a,b), atomic anisotropic displacement parameters (Table S5a,b), and hydrogen atoms positions (Table S6a,b). Table S7 including a comparison of  $^{13}\text{C}$  NMR chemical shifts of complexes and free ligands.

## References

- (1) [http://www.who.int/topics/infectious\\_diseases/en/](http://www.who.int/topics/infectious_diseases/en/) (visited 8/12/2014)
- (2) <http://www.who.int/chagas/en/> (visited 8/12/2014)
- (3) I. Ribeiro, A.M. Sevcsik, F. Alves, G. Diap, R. Don, M.O. Harhay, S. Chang, B. Pecoul, *PLoS Negl. Trop. Dis.* 2009, **3**, e484, doi:10.1371/journal.pntd.0000484.

- (4) J.A. Urbina, *Drugs Future* 2010, **35**, 409-419.
- (5) J.D. Maya, B.K. Cassels, P. Iturriaga-Vásquez, J. Ferreira, M. Faúndez, N. Galanti, A. Ferreira, A. Morello, *Comp. Biochem. Physiol. Part A* 2007, **146**, 601-620.
- (6) A. Rassi, A. Rassi, J.A. Marin-Neto, *Lancet* 2010, **375**, 1388-1402.
- (7) <http://www.who.int/topics/tuberculosis/en/> visited 8/12/2014
- (8) WHO Global Tuberculosis Report 2013.
- (9) A. Zwerling, M. A. Behr, A. Verma, T. F. Brewer, D. Menzies, M. Pai, *Plos Medicine* 2011, **8**, doi: 10.1371/journal.pmed.1001012
- (10) N. R. Gandhi, P. Nunn, K. Dheda, H.S. Schaaf, M. Zignol, D. van Soolingen, P. Jensen, J. Bayona, *Lancet* 2010, **375**, 1830-1843.
- (11) Z. Ma, C. Lienhardt, H. McIlleron, A. J Nunn, X. Wang, *Lancet* 2010, **375**, 2100-2109.
- (12) R. P. Tripathi, N. Tewari, N. Dwivedi, V. K. Tiwari, *Med. Res. Rev.* 2005, **25**, 93-131.
- (13) D. Gambino, L. Otero, *Inorg. Chim. Acta* 2012, **393**, 103-114.
- (14) M. Navarro, G. Gabbiani, L. Messori, D. Gambino, *Drug Discov. Today* 2010, **15**, 1070-1078.
- (15) J. Costa Pessoa, S. Etcheverry, D. Gambino, *Coord. Chem. Rev.* <http://dx.doi.org/10.1016/j.ccr.2014.12.002>
- (16) I. Machado, L. Biancolino Marino, B. Demoro, G. A. Echeverría, O. E. Piro, C. Q. F. Leite, F. R. Pavan, D. Gambino, *Eur. J. Med. Chem.* 2014, **87**, 267-273.
- (17) M. Poggi, R. P. Barroso, A. J. Costa-Filho, H. Barbosa de Barros, F. R. Pavan, C. Q.F. Leite, D. Gambino, M. H. Torre, *J. Mexican Chem. Soc.* 2013, **57**, 198-204.
- (18) M. B. Tarallo, C. Urquiola, A. Monge, B. Parajón Costa, R. R. Ribeiro, A. J. Costa-Filho, R. C. Mercader, F. R. Pavan, C. Q. F. Leite, M. H. Torre, D. Gambino, *J. Inorg. Biochem.* 2010, **104**, 1164–1170.

- (19) M. B. Tarallo, A. J. Costa-Filho, E. D. Vieira, A. Monge, C. Q. Leite, F. R. Pavan, G. Borthagaray, D. Gambino, M. H. Torre, *J. Argentine Chem. Soc.* 2009, **97**, 80-89.
- (20) M. Vieites, P. Smircich, B. Parajón-Costa, J. Rodríguez, V. Galaz, C. Olea-Azar, L. Otero, G. Aguirre, H. Cerecetto, M. González, A. Gómez-Barrio, B. Garat, D. Gambino, *J. Biol. Inorg. Chem.* 2008, **13**, 723-735.
- (21) M. Vieites, P. Smircich, L. Guggeri, E. Marchán, A. Gómez-Barrio, M. Navarro, B. Garat, D. Gambino, *J. Inorg. Biochem.* 2009, **103**, 1300-1306.
- (22) A. Merlino, M. Vieites, D. Gambino, E. L. Coitiño, *J. Mol. Graphics Mod.* 2014, **48**, 47-59.
- (23) J.F. Turrens, C.L. Newton, L. Zhong, F.R. Hernández, J. Whitfield, R. Docampo, *FEMS Microbiol. Lett.* 1999, **175**, 217-221.
- (24) S. Watanabe, M. Zimmermann, M. B. Goodwin<sup>1</sup>, U. Sauer, C. E. Barry, H. I. Boshoff, *PLoS Pathogens* 2011, **7**, e1002287.
- (25) R.H. Fish, G. Jaouen, *Organometallics* 2003, **22**, 2166-2177.
- (26) C. Biot, *Curr. Med. Chem. - Anti-Infective Agents* 2004, **3**, 135-147.
- (27) C. Biot, D. Dive, *Top. Organomet. Chem.* 2010, **32**, 155-193.
- (28) T.A.K. Al-Allaf, H. Schmidt, K. Merzweiler, C. Wagner, D. Steinborn, *J. Organometal. Chem.* 2003, **678**, 48 - 55.
- (29) W. J. Geary, *Coord. Chem. Rev.* 1971, **7**, 81-91.
- (30) CrysAlisPro, Oxford Diffraction Ltd., version 1.171.33.48 (release 15-09-2009 CrysAlis171.NET).
- (31) G. M. Sheldrick, *Acta Crystallogr.* 2008, **A64**, 112-122.
- (32) J.C. Palomino, A. Martin, M. Camacho, H. Guerra, J. Swings, F. Portaels, *Antimicrob. Agents Chemother.* 2002, **46**, 2720-2722.
- (33) J. Benítez, L. Becco, I. Correia, S. Milena Leal, H. Guiset, J. Costa Pessoa, J. Lorenzo, S. Tanco, P. Escobar, V. Moreno, B. Garat, D. Gambino, *J. Inorg. Biochem.* 2011, **105**, 303-312.

- (34) M. Fernández, L. Becco, I. Correia, J. Benítez, O. E. Piro, G. A. Echeverria, A. Medeiros, M. Comini, M. L. Lavaggi, M. González, H. Cerecetto, V. Moreno, J. Costa Pessoa, B. Garat, D. Gambino, *J. Inorg. Biochem.* 2013, **127**, 150-160.
- (35) F. R. Pavan, P.I. da S. Maia, S.R. Leite, V. M. Deflon, A. A. Batista, D.N. Sato, S.G. Franzblau, C.Q. Leite, *Eur. J. Med. Chem.* 2010, **45**, 1898-1905.
- (36) P.B. Christmas, J.F. Turrens, *FEMS Microbiol Letters* 2000, **183**, 225-228.
- (37) A.D. Becke, *Phys. Rev. A* 1988, **38**, 3098-3100.
- (38) J. P. Perdew, *Phys. Rev. B* 1986, **33**, 8822-8824.
- (39) W. J. Hehre, L. Random, P. v. R. Schleyer, and J. A. Pople, "Ab Initio Molecular Orbital Theory", Wiley, New York, 1986.
- (40) B. J. Lynch, Y. Zhao, D. G. Truhlar, *J. Phys. Chem. A* 2003, **107**, 1384-1388.
- (41) P.J. Hay, W.R. Wadt, *J. Chem. Phys.* 1985, **82**, 270-283; *ibid*, pp. 299-310.
- (42) A. E. Reed, L. A. Curtiss, F. Weinhold, *Chem. Rev.* 1988, **88**, 899-926.
- (43) I. Mayer, *J. Comput. Chem.* 2007, **28**, 204-221.
- (44) M. J. Frisch, G. W. Trucks, H. B. Schlegel, G. E. Scuseria, M. A. Robb, J. R. Cheeseman, G. Scalmani, V. Barone, B. Mennucci, G. A. Petersson, *et al.*, "Gaussian 09, Rev. A.02", Gaussian Inc., Wallingford, CT, USA, 2009.
- (45) G.M. Morris, R. Huey, W. Lindstrom, M.F. Sanner, R.K. Belew, D.S. Goodsell, A.J. Olson, *J. Comput. Chem.* 2009, **30**, 2785-2791.
- (46) Autodock Forum. ADL, Parameters for docking with metal ions in receptor, 2009 (accessed December, 2004). <http://autodock.1369657.n2.nabble.com/ADL-Parameters-for-docking-with-metal-ions-in-receptor-td2505649.html>
- (47) A. Divsalar, A.A. Saboury, L. Ahadi, E. Zemanatiyar, H. Mansouri-Torshizi, D.Ajloo, R.H. Sarma, *J. Biomol. Struct. Dyn.* 2011, **29**, 283-296.
- (48) L. J. Farrugia, *J. Appl. Cryst.* 1997, **30**, 565-566.

- (49) T. Hayashi, M. Konishi, Y. Kobori, M. Kumada, T. Higuchi, K. Hirotsu, *J. Am. Chem. Soc.* 1984, **106**, 158-163.
- (50) J-H Zhou, Y-Z Li, Z. Liu, X-T Chen, *Acta Cryst.* 2005, E61, m195-m197.
- (51) J. C. Shi, T.B. Wen, Y. Zheng, S.J. Zhong, D.X. Wu, Q.T. Liu, B. S. Kang, B. M. Wu, T. C. Mak, *Polyhedron* 1997, **16**, 369–375.
- (52) A. Togni, T. Hayashi “Ferrocenes: Homogeneous Catalysis, Organic Synthesis, Materials Science” Weinheim - New York Basel - Cambridge. Tokyo, 1995.
- (53) C. E. Housecroft, S. M. Owen, P. R. Raithby, B. A. M. Shaykh, *Organometallics* 1990, **9**, 1617- 1623.
- (54) D. Cauzzi, C. Graiff, C. Massera, G. Predieri, A. Tiripicchio, D. Acquotti, *J. Chem. Soc., Dalton Trans.* 1999, 3515–3521.
- (55) S. A. Al-Jibori, A. I.A. Al-Nassiry, G. Hogarth, L. Salassa, *Inorg. Chim. Acta* 2013, **398**, 46–53.
- (56) S. A. Ramírez, G. J. Gordillo, *J. Electroanalytical Chem.* 2009, **629**, 147–151.
- (57) E.R. Brown, R.F. Large (1971) In: Weisberger A, Rositer BW (eds) Part IIA, Chapter 6. Interscience, New York.
- (58) Handbook of anti-tuberculosis agents. *Tuberculosis* 2008, **88**, 85-169.
- (59) D. Gambino, M. Fernández, D. Santos, G. A. Etcheverría, O. E. Piro, F. R. Pavan, C. Q. F. Leite, I. Tomaz, F. Marques, *Polyhedron* 2011, **30**, 1360-1366.
- (60) I. Orme, *Antimicrob Agents Chemother.* 2001, **45**, 1943-1946.
- (61) P. Dans, E.L. Coitiño, *J. Chem. Inf. Modeling* 2009, **49**, pp. 1407–1419.
- (62) A. Merlino, L. Otero, D. G. Gambino, E. L. Coitiño, *Eur. J. Med. Chem.* 2011, **46**, 2639–2651.